V61

Helium-Neon Laser

Christopher Breitfeld
christopher.breitfeld@tu-dortmund.de

Henry Krämerkämper
henry.kraemerkaemper@tu-dortmund.de

Durchführung: 23. October 2023 Abgabe: February 15, 2024

TU Dortmund – Fakultät Physik

Contents

1 Aims of the Experiment

The objective of V61 is to conduct a comprehensive investigation of a Helium-Neon (HeNe) laser. This involves the analysis of two transverse electromagnetic (TEM) modes and the evaluation of its stability conditions. Additionally, it encompasses the determination the laser's polarization state and wavelength.

2 Theoretical Description of the functionality of a Laser

A laser (Light Amplification by Emission of Radiation) comprises three essential components. These components include a laser medium, which in this instance is a gas mixture of helium and neon, a pump source, specifically an electric discharger and an optical resonator, in this case one partially and one fully reflecting mirror. The laser medium is responsible for the laser's radiation spectrum, primarily due to its specific excitation energy. In the case of a HeNe laser, the active laser medium is the noble gas neon. This laser medium possesses various energy states, enabling three fundamental processes, as illustrated in Figure 1. If the atom is in the ground state, it can absorb a photon with the required energy for excitation, resulting in the atom having one electron at a higher energy level. This process is known as absorption. An excited atom can spontaneously transition back to the lower energy ground state, emitting a photon with the remaining energy, in line with energy conservation. The direction of the emitted photon is random. This process is called spontaneous emission. Another de-excitation process is stimulated emission. In this case an excited atom is struck by a photon with precisely the same energy as the difference between the excited and ground state. This causes the atom to emit a photon and return to the ground state. The incoming and emitted photons have the same energy, direction and phase, making them coherent. In contrast to the

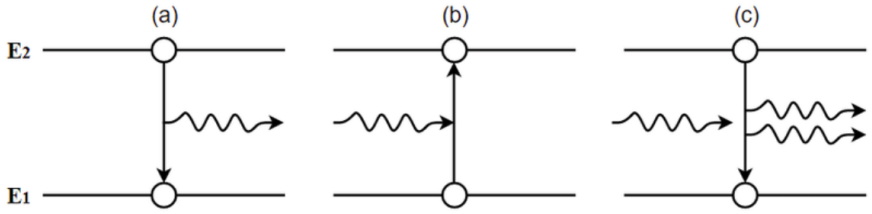

Figure 1: Diagrammatic representation of absorption (a), spontaneous emission (b), and stimulated emission (c) for a two-state system. [1]

illustration in Figure 1, a laser requires a laser medium with more than two energy levels. In a two level system, the Einstein coefficients B_{12} and B_{21}, which describe the transition probability between states, are equal. Due to this, the population inversion necessary for the laser is not achievable in a tow-level system. To achieve population inversion, a pump source must input energy into the system. In the case of a HeNe laser, an electric discharger pumps energy into the pump gas helium. The excited helium atoms collide with neon atoms, transferring their energy. The level diagram is illustrated in Figure 2.

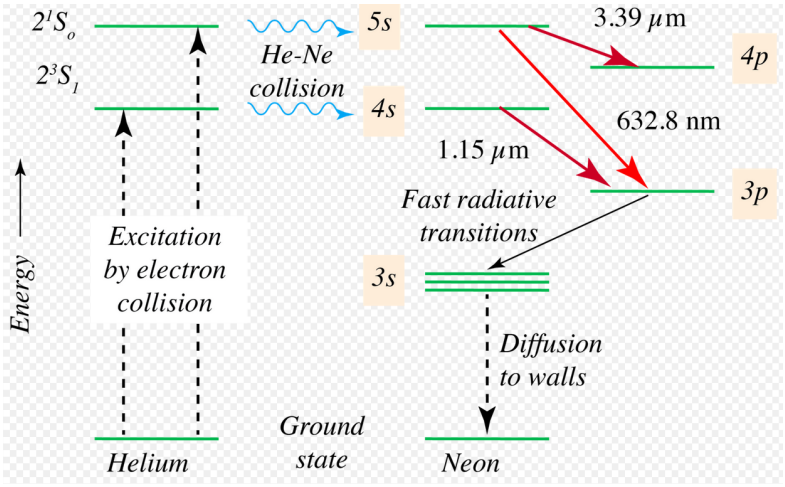

Figure 2: Diagrammatic representation of the level schema for the HeNe lasers. [4]

The transition from the 3s to the p2 state predominates the process, resulting in the production of red laser light with a wavelength of $\lambda = 632.8\,\text{nm}$. As amplification is dependent on the distance travelled, a resonator is employed to increase the path length. This is implemented using two mirrors, one fully reflecting and one partially reflecting, enabling the beam to exit the laser tube in one direction. To control the laser, the resonator must satisfy the stability relation

$$0 < g_1 g_2 \leq 1 \tag{1}$$

where $g_i = 1 - \frac{L}{r_i}$ is defined with the length L and the curvature radius r_i of the mirror i. If condition (1) is not met, the laser beam may grow until it becomes larger than the mirror, resulting in its loss. Figure 3 displays two resonators, one stable and one unstable.

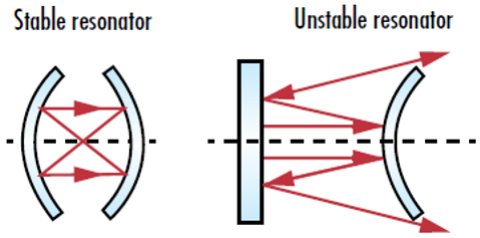

Figure 3: Graphical illustration of the beam path in one resonator that fulfils the stability condition (1) (left) and an unstable resonator (right). [3]

The light forms standing waves between the mirrors, denoted as TEM_{pl}, where p and l describe the radial and angular mode orders. Figure 4 shows the patterns of the first orders.

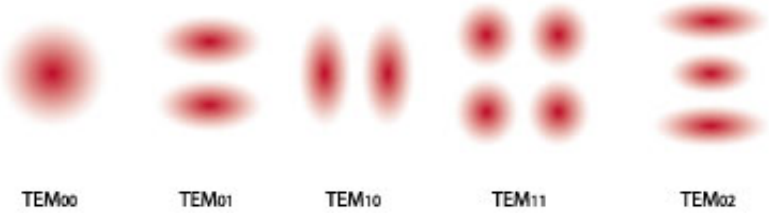

Figure 4: The intensity distribution of the laser modes TEM_{00}, TEM_{01}, TEM_{10}, TEM_{11} and TEM_{02}. [2]

The amplitude of the mode TEM_{pl} is described by

$$A_{pl}(x,y) = \mathrm{H}_l(x)\mathrm{H}_m(y)\exp -(x^2+y^2) \tag{2}$$

where H_i represents the Hermite polynomial of order i. The absolute square $|A_{pl}(x,y)|^2$ corresponds to the intensity $I_{pl}(x,y)$.

3 Experimental Setup and Measurements

As explained in Section 2, the primary laser consists of three essential components. These include the laser tube, filled with laser medium, the resonator, which is constructed with one partially reflecting and one fully reflecting mirror, and the pump source, represented in this case electrodes. Before using the laser, it requires adjustment. To accomplish this, an alignment laser ($\lambda = 532\,\mathrm{nm}$) with a power of $P_{\mathrm{green}} = 0.2\,\mathrm{W}$ and a target screen are positioned at the end of the optical bench. The alignment laser should be aligned with the optical axis of the main laser so that it intersects with the holes in the target screen of the primary laser. At the end of the laser tube, Brewster windows are positioned. These optical components enable the control of light polarization by minimizing the reflectance of one polarization at a specific angle of incidence, known as the Brewster angle. Figure 5 illustrates how a Brewster window operates.

3.1 Examination of the Stability Condition

To examine the stability condition, the resonator length is increased while measuring the laser intensity with a photodiode. This procedure is performed for different mirrors with varying curvature radii.

3.2 Observation of the TEM Modes

To examine the different modes, a wire (diameter $d = 0.005\,\mathrm{mm}$) is positioned between the laser tube and the mirror. After expanding the beam with a scattering lens, modes can be identified on the screen. Then the screen is replaced with a photodiode to measure the intensity distribution. This procedure is repeated for two modes.

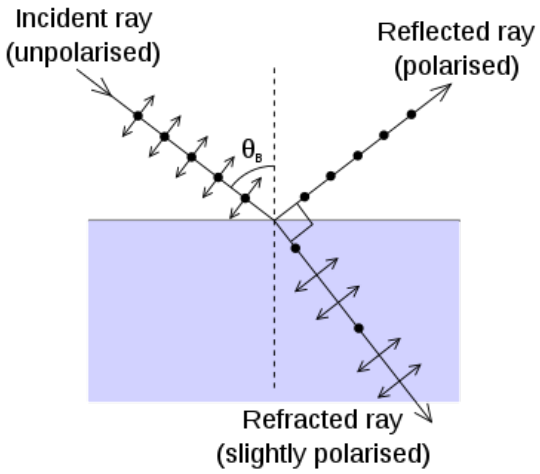

Figure 5: Light path of perpendicularly and parallel polarized light directed at an interface at the Brewster angle θ_B. [5]

3.3 Determination of the Polarisation

To measure the intensity dependence on the polarization direction, a polarizer is positioned between the laser and the photodiode. This polarizer is used to set the polarization direction to be measured.

3.4 Multi-mode Operation and Frequency Spectrum of the Laser

A high-speed photodiode (bandwidth up to 1 GHz) is utilized to measure the beat frequencies for various resonator length. The Fourier spectra are subsequently analysed using a spectrum analyser.

3.5 Determining the Wavelength

To determine the wavelength of the laser, various gratings and slits are positioned in the beam. The distance between the diffraction maxima is subsequently measured.

4 Analysis

4.1 Measurement of the stability condition

As described in Chapter 2, in order to achieve a stable resonator for laser emission, the stability condition 1 must hold true. The two mirror configurations available are Flat/Flat-Flat/1400 mm and Flat/1400 mm-Flat/1400 mm. The stability condition 1 yields a maximum resonator length of $L_1 = r_2 = 1400\,\text{mm}$ for the former and $L_2 = r_1 + r_2 = 2800\,\text{mm}$ for the later configuration. To test these theoretical calculations, the achieved laser intensity in different mirror and length configurations is measured. The resulting data is displayed in Figure 6.

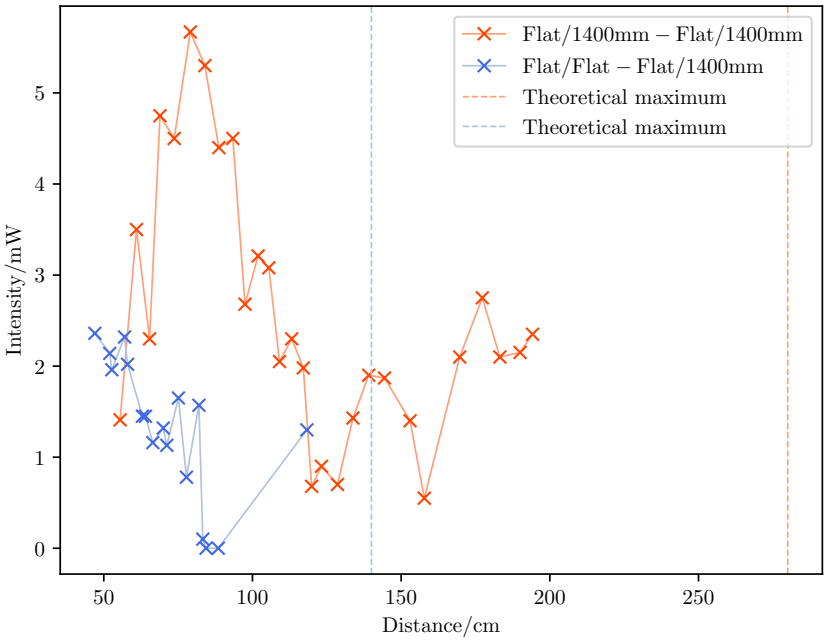

Figure 6: Plot of the intensity measurement for different resonator configurations.

The data is given in tabular form in Table 1. The measurement was carried out until a consistent intensity measurement was not possible or the length of the optical bench was reached.

Table 1: Measurements of the Laser intensity for different resonator lengths and mirror configurations.

Flat/1400mm-Flat/1400mm		Flat/Flat-Flat/1400mm	
d/cm	I/mW	d/cm	I/mW
63.5	1.41	55.0	2.36
69.0	3.50	60.0	2.14
73.4	2.30	60.7	1.96
76.9	4.75	65.0	2.32
81.7	4.5	66.0	2.02
87.1	5.67	71.0	1.45
92.0	5.3	72.0	1.45
96.7	4.4	74.5	1.16
101.4	4.5	78.0	1.32
105.5	2.68	79.2	1.13
109.9	3.21	83.1	1.65
113.5	3.08	85.8	0.78
117.1	2.05	90.0	1.57
121.2	2.3	91.3	0.1
125.1	1.98	92.4	0
127.9	0.68	96.5	0
131.2	0.9	126.3	1.3
136.6	0.7		
141.8	1.43		
147.1	1.9		
152.4	1.87		
161.0	1.4		
165.8	0.55		
177.7	2.1		
185.3	2.75		
191.2	2.1		
198.0	2.15		
202.2	2.35		

4.2 TEM Modes

In this section, the TEM_{00} and TEM_{10} modes described in 2 are observed by measuring the laser intensity perpendicular to the optical axis. The measurement accuracy is estimated to be $\sigma_I = 0.09\,\mathrm{mW}$.

4.2.1 TEM_{00} Mode

The amplitudes of the Modes are given by Equation (2). Therefore the intensity of the TEM_{00} mode is described by

$$I = I_{\max} \cdot \exp\left(\frac{-(r - r_0)^2}{2\omega^2}\right) + I_0. \tag{3}$$

Here, $I_{\max}$ denotes the maximum intensity, I_0 the intensity contribution by background light, r_0 the centre of the laser beam and ω describes the width of the gaussian curve. Measurement of the background light with the laser being deactivated yielded an intensity of $I_0 = 0.0001\,\mu\mathrm{A}$. The parameters of (3) are fitted to the measurements using `scipy.optimize.curve_fit`; the resulting values are shown below.

$$\begin{aligned} I_{\max} &= (9.04 \pm 0.22)\,\mu\mathrm{A} \\ r_0 &= (8.67 \pm 0.13)\,\mathrm{cm} \\ \omega &= (4.72 \pm 0.13)\,\mathrm{cm}. \end{aligned}$$

The fitted curve and the data is displayed in Figure 7.

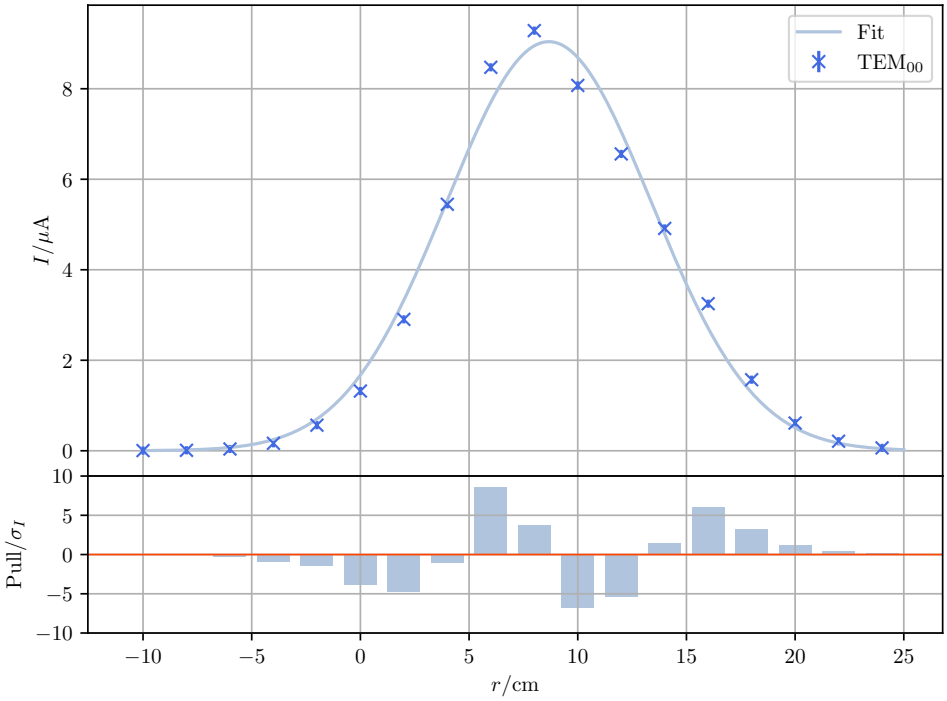

Figure 7: Intensity measurement of the TEM_{00} mode.

4.2.2 TEM_{01} Mode

The intensity of the TEM_{10} is given by equation (4)

$$I = I_{\max} \cdot \frac{4(r - r_0)^2}{\omega^2} \cdot \exp\left(\frac{-(r - r_0)^2}{2\omega^2}\right) + I_0. \tag{4}$$

Equation (4) is again fitted to the measured data using `scipy.optimize.curve_fit`, which yields the parameters

$$\begin{aligned} I_{\max} &= (0.91 \pm 0.02)\,\mu\mathrm{A} \\ r_0 &= (6.54 \pm 0.10)\,\mathrm{cm} \\ \omega &= (4.71 \pm 0.07)\,\mathrm{cm}. \end{aligned}$$

The resulting curve is depicted in Figure 8.

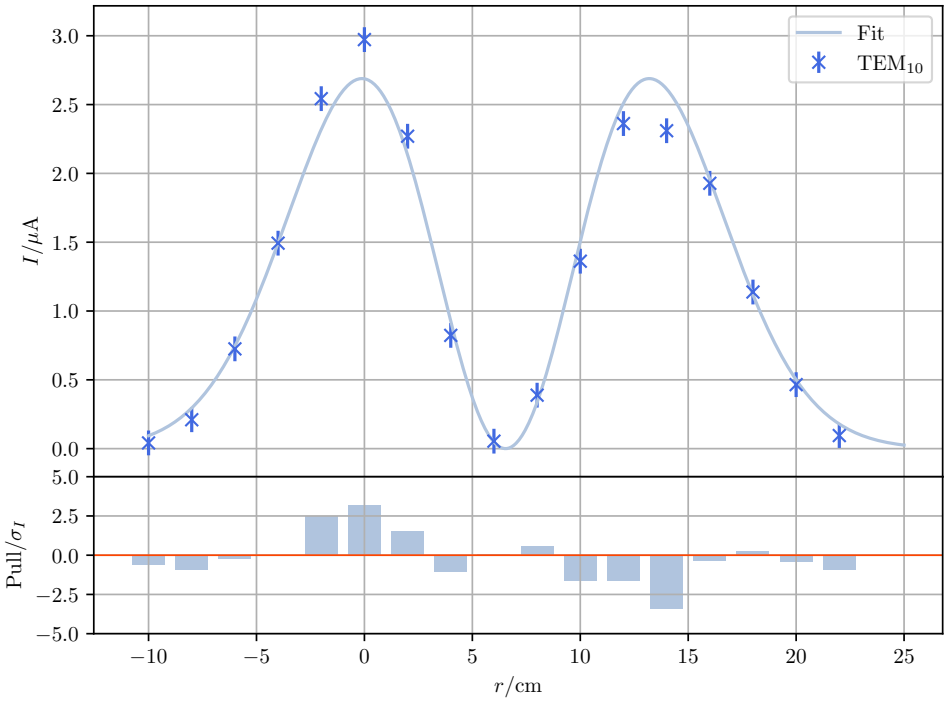

Figure 8: Intensity measurement of the TEM_{10} mode.

4.3 Polarisation of the laser

The Brewster windows mentioned in Section 3 ensure that most light passing through is p-polarised. To verify this, a measurement of the intensity dependence on the polarisation angle is carried out. The theoretical intensity curve is given by Equation (5)

$$I = I_{\max} \cdot \sin(\alpha + \alpha_0)^2 + I_0, \tag{5}$$

where I_{max} describes the maximum intensity, α_0 the zero angle and I_0 again describes the intensity contribution by background light. Using `scipy.optimize.curve_fit`, this function is fitted to the measured data. The results are shown in Figure 9. The resulting

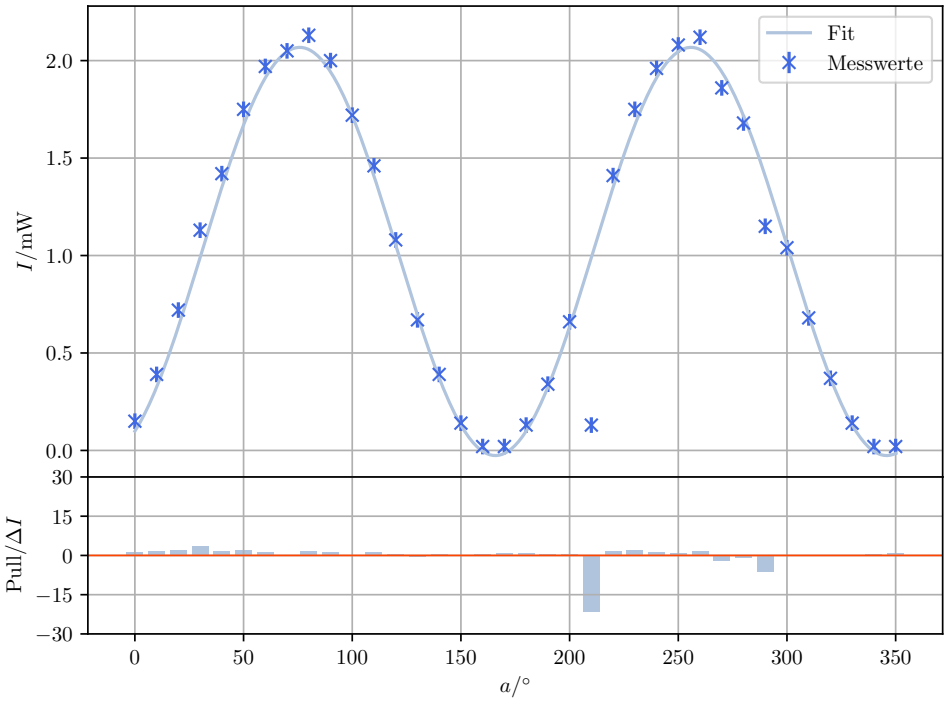

Figure 9: Intensity measurement for different polarisation filter angles.

fit parameters are

$$I_{\text{max}} = (2.09 \pm 0.08)\,\text{mW}$$
$$I_0 = (-0.03 \pm 0.05)\,\text{mW}$$
$$\alpha_0 = (194.15 \pm 1.06)°.$$

The measured data is given in tabulary form in Table 2.

Table 2: Measurements of the Laser intensity for different angles.

$\alpha/°$	I/mW	$\alpha/°$	I/mW
0	0.15	180	0.13
10	0.39	190	0.34
20	0.72	200	0.66
30	1.13	210	0.13
40	1.42	220	1.41
50	1.75	230	1.75
60	1.97	240	1.96
70	2.05	250	2.08
80	2.13	260	2.12
90	2.00	270	1.86
100	1.72	280	1.68
110	1.46	290	1.15
120	1.08	300	1.04
130	0.67	310	0.68
140	0.39	320	0.37
150	0.14	330	0.14
160	0.02	340	0.02
170	0.02	350	0.02

4.4 Examination of the frequency spectrum of the laser

To measure the frequency spectrum of the Helium-Neon-Laser in multi-mode operation, a fast photodiode connected to an oscilloscope is utilized. The measurement is carried out for four different resonator lengths. The distance between the peak frequencies is used to compare it to the theoretical mode distance given by (6):

$$\Delta f_{\mathrm{Theory}} = \frac{c}{2 \cdot L}. \tag{6}$$

Therefore, each mode difference has to be an integer multiple of $\Delta f_{\mathrm{Theory}}$:

$$f_{\mathrm{Theory}} = n \cdot \Delta f_{\mathrm{Theory}} = n \cdot \frac{c}{2 \cdot L}. \tag{7}$$

The resulting data is given in Table 3.

Table 3: Measurements of the Laser spectrum in multi-mode operation for different resonator lengths.

Peak	f/MHz			
	$L = 87.5\,\text{cm}$	$L = 66.8\,\text{cm}$	$L = 156.5\,\text{cm}$	$L = 215.8\,\text{cm}$
1	188	255	105	221
2	379	518	206	439
3	570	773	308	653
4	758	1031	405	870
5	949		510	1084
6	1140		608	1305
7			709	
8			814	
9			911	
10			1016	
11			1114	
12			1219	
13			1320	

In Table 4, the mean of the deltas between the peaks for each of the four lengths are displayed and compared to the closest theoretical mode distance.

Table 4: Comparison between the mean measured frequency deltas and the theoretical values for different resonator lengths.

L/cm	$\bar{\Delta}f$/MHz	Δf_{Theory}	$\bar{\Delta}f - \Delta f_{\text{Theory}}$	$(\bar{\Delta}f - \Delta f_{\text{Theory}})/\%$
87.5	190.40	171.3	19.1	11.15
66.8	258.67	224.4	34.27	15.27
156.5	101.25	95.78	5.47	5.71
215.8	216.80	69.46	147.34	212.12

The spectrum resulting from the Neon-transition is widened by the Doppler-effect. The frequency change δf resulting from the linear Doppler-effect can be calculated by (8):

$$\delta f = \frac{f_0}{c}\sqrt{\frac{8k_B T \log(2)}{m}}. \tag{8}$$

With $T = 19\,^{\circ}\text{C} = 292.2\,\text{K}$, $m = 3.3509 \times 10^{-26}\,\text{kg}$ and a Laser frequency of $f_0 = \frac{\lambda}{c} = 4.74 \times 10^5\,\text{GHz}$, the resulting frequency shift is given by (9):

$$\delta f = 1292\,\text{MHz}. \tag{9}$$

The Doppler shift therefore is approximately 6, 5, and 12 times $\bar{\Delta}f$ of the measurements for first three resonator lengths.

4.5 Laser wavelength

To determine the laser wavelength, the diffraction maxima for several different optical gratings are measured. The wavelength can be determined by utilizing the relation (10).

$$k\lambda = d\sin(\alpha_k) \Rightarrow \lambda = \frac{d \cdot a_k}{k\sqrt{e^2 + a_k^2}}. \tag{10}$$

Here, d describes the distance between the slits of the optical grating, e is the distance between the optical grating and the screen and a_k describes the distance between the optical axis and the diffraction maximum with order k. The measured values of a_k for different optical gratings are displayed in Table 5. The first two measurements were carried out with a distance $d = 70\,\text{cm}$ and the last two with a distance $d = 29.4\,\text{cm}$.

Table 5: Measurements of a_k for different optical gratings.

	a_k/cm			
$2k$	80l/mm	100l/mm	600l/mm	1200l/mm
1	7.1	9.0	24.0	68.5
2	14.3	18.2	44.6	
3	21.5	27.4		
4	32.8	37.0		
5	40.6	47.1		
6	44.5	63.3		

The measurements in Table 5 are taken from the k-maximum on one side of the optical axis to the k-maximum on the other side of the optical axis and then halfed in the computation of λ to reduce the uncertainty of the measurement. The remaining measurement uncertainty is estimated to be $\sigma_{a_k} = 0.2\,\text{cm}$. Using Equation (10), the following wavelengths were obtained:

$$\begin{aligned}
\lambda_1 &= (660.6806 \pm 3.6321)\,\text{nm} \\
\lambda_2 &= (664.8679 \pm 2.6663)\,\text{nm} \\
\lambda_3 &= (515.2400 \pm 1.9317)\,\text{nm} \\
\lambda_4 &= (632.3227 \pm 0.7832)\,\text{nm}.
\end{aligned}$$

The average wavelength resulting of all four measurements weighted by their respective uncertainty is given by

$$\bar{\lambda} = (620.6652 \pm 1.3754)\,\text{nm}. \tag{11}$$

5 Conclusion

The stability condition could not be thoroughly assessed due to certain limitations encountered during the experiment. Firstly, the physical length of the optical bench

constrained the verification of the theoretical maximum during the measurement of the first mirror configuration. Secondly, during the measurement of the second configuration, the adjustment quality of the laser varied and led to suboptimal results and prevented a measurement for higher distances altogether. In both instances, it was not possible to reach the theoretical limits. Enhancements in the experimental setup could be made to overcome these challenges. Utilizing a longer optical bench and implementing a method that allows for the mirrors' repositioning without compromising their alignment could lead to a more consistent alignment across varying resonator lengths.

The measurement of the TEM-Modes could be done with sufficient accuracy, as both fits show little deviation from the measured data (see Figure 7, 8). The uncertainties in the fit parameters as well as the estimated measurement uncertainty of $\sigma_I = 0.09\,\mu\text{A}$ collectively do not exceed $2.4\,\%$.

The laser polarization exhibits the expected periodicity of 2π, with only minor deviations from the fit compared to the actual data, which can be seen in Figure 9. The discrepancies are likely attributed to fluctuations that made it difficult reading of the instrument. Moreover, the observed phase shift is presumably due to the imperfect parallel alignment of the laser.

The measurement of the longitudinal modes shows satisfactory accuracy in the initial three measurements. A linear scaling of accuracy with the number of data points appears evident from the observations for the first three resonator lengths. Limited statistics seem to be the biggest challenge in this context, contributing to discrepancies in the results. Additionally, the last measurement seems to be corrupted by the increased length of the resonator and the resulting difficulties in the adjustment process. This leads to a more substantial deviation from the theoretical values, which can be seen in Table 4. Therefore, this measurement should be excluded.

The examination of the laser wavelength seems to be reasonably accurate. The weighted average $\bar{\lambda} = (620.6652 \pm 1.3754)\,\text{nm}$ deviates from the theoretical value of $\lambda_{\text{Theory}} = 632.8\,\text{nm}$ by $(1.92 \pm 0.28)\,\%$. The remaining deviation is most likely caused by the screen not being perfectly orthogonal to the optical axis as well as imprecise measurements because of the need of darkening the room. Using a more sophisticated device to measure distances than a normal tape measure, even better results could probably be achieved. Also increasing the width of the screen would allow more orders of diffraction to be measured, which could increase the accuracy of the measurement, especially for the later two.

References

[1] Hassan El-Henawi. "Simulation, Fabrication, and Characterization of Optically Pumped Semiconductor Disk Lasers Without Substrate Removal". PhD thesis. Aug. 2019. DOI: 10.13140/RG.2.2.20281.93281.

[2] *Laser Modes*. 2021. URL: https://scitec.uk.com/lasers/laser_modes.php (visited on 10/24/2023).

[3] *Laserresonator und Resonatormoden*. 2023. URL: https://www.edmundoptics.de/knowledge-center/application-notes/lasers/laser-resonator-modes/ (visited on 10/17/2023).

[4] *Wikipedia. Helium-neon laser*. 2023. URL: https://en.wikipedia.org/wiki/Helium%E2%80%93neon_laser (visited on 10/17/2023).

[5] *Wikipedia. Brewster's angle*. 2023. URL: https://en.wikipedia.org/wiki/Brewster%27s_angle (visited on 10/17/2023).